Wall Shear Stress and Atherosclerosis: Numerical Blood Flow Simulations in the Mouse Aortic Arch

P. RUENGSAKULRACH [a,b,c,f], A. K. JOSHI[b], S. FREMES[c], S. FOSTER[d], J. BUTANY[e], B. WIWATANAPATAPHEE[a], Y. LENBURY[a]

[a] Department of Mathematics
Mahidol University, Faculty of Science, Rama 6 Road, Bangkok 10400
THAILAND
[b] Department of Mechanical and Industrial Engineering
[c] Division of Cardiac and Vascular Surgery and [d] the Imaging Research Centre for Cardiac Intervention
Sunnybrook Health Sciences Centre
[e] Department of Pathology
Toronto General Hospital
The University of Toronto, 5 King's College Road, Toronto, Ontario
CANADA
[f] Bangkok Heart Hospital
2 Soi Soonvijai 7, New Petchburi Road, Bangkok 10320
THAILAND

permyos@bangkokheart.com

Abstract: - The aims of this study were (1) to demonstrate the feasibility of computational fluid dynamic (CFD) modelling of realistic blood flow in the mouse aortic arch, and (2) to determine the relation of wall shear stress and atherosclerosis in the mouse aortic arch. ApoE knockout mice were chosen for this study. The blood flow fraction in the major branches of the mouse aortic arch was measured by ultrasound biomicroscopy. The geometry of the aortic arch was captured by plastic casting and micro CT imaging. Mouse blood viscosities were measured by rheometry. A pathological examination was performed. A well-validated in-house finite element code, which solves the three dimensional Navier-Stokes equations, was used to compute the wall shear stress and velocity patterns in the ascending aorta and the aortic arch. The distribution of the wall shear stress was correlated with the distribution of the atherosclerosis from the pathological examination in order to investigate the effect of wall shear stress on atherosclerosis. It is concluded that CFD modeling of hemodynamics in the mouse aortic arch is feasible. Qualitative impressions show that atherosclerosis was related with the region of low wall shear stress in mouse aortic arch.

Key-Words: - Blood Flow, Mouse, Aortic Arch, Wall Shear Stress, Atherosclerosis

1 Introduction

Atherosclerosis is a major disease, causing blockage of arteries throughout the body including coronary artery, cerebral artery and peripheral arteries leading to myocardial ischemia/infarction, stroke and claudication, respectively. Shear stress in arteries is associated with the pathophysiology of atherosclerosis. Mouse was chosen for this study because of its small size, relatively low maintenance costs, rapid gestation and large litter size. Extensive knowledge of the mouse genome exists. Genetically engineered mice are potential models for studying changes in advanced atherosclerotic lesions, which may cause stenosis. Of all the models of mouse atherosclerosis, the apolipoprotein E knock-out mouse (apoE-/-) has been studied the most extensively for the effects of genetic and pharmacological interventions on the development of lesions. A deficiency of the apolipoprotein E gene (apoE-/-) mice results in hypercholesterolemia with the formation of lesions strikingly similar to those found in

humans. This experimental model overcomes many limitations of human studies, e.g. invasive intervention, tissue sample and study time. We also chose to study the blood flow in mouse aortic arch as it has complex geometry and has the greatest diameter/ size in a mouse. To study blood flow and atherosclerosis in mouse aortic arch, the real geometry of artery, blood viscosity, flow and pathology are required.

The aims of this work were (1) to demonstrate the feasibility of computational fluid dynamic (CFD) modelling of realistic blood flow in the mouse aortic arch, and (2) to determine the relation between wall shear stress to atherosclerosis in the mouse aortic arch.

2 Method

All procedures described below complied with the standards for care and use of animal subjects as stated in the Guide for the Care and Use of Laboratory Animals (The Canadian Council on Animal Care, the requirements under the Animals for Research Act, RSO 1980, and Sunnybrook & Women's Animal Care Committee Policies and Guidelines). Atherosclerosis was induced in 15 apolipoprotein E knock-out mice (apoE-/-) (experiment), age 15 weeks, by a high cholesterol diet for 4-8 weeks. Five apoE knockout mice (control) were fed a normal diet. Twenty normal mice served as normal control.

2.1 Hemodynamic measurements

The ultrasound biomicroscope (model VS40; VisualSonics, Toronto, Canada) was used for measuring blood flow in the mouse aorta and arteries. The biomicroscope has a single transducer with a nominal center frequency of 30 MHz, a diameter of 3 mm, and a focal length of 6 mm. Light general anaesthesia was induced with isoflurane in oxygen by face mask and mice were kept warm using a thermo-controlled heating pad and heat lamp. Heart rate and rectal temperature of mice was monitored (model THM100; Indus Instruments, Houston, TX). The rectal temperature was kept at 37°C. The neck, chest and abdomen was shaved, prepped and treated with a chemical hair remover to minimize ultrasound attenuation. After prewarming the ultrasound gel, an outer ring of thick gel (Aquasonic 100; Parker Laboratories, Orange, NJ) was filled with a thinner gel (EcoGel 100; Eco-Med Pharmaceutical, Mississauga, Ontario, Canada) over the region of interest, to provide an acoustic coupling medium. All mice had their ascending aorta, innominate artery, left common carotid artery, and subclavian artery examined by the multifrequency ultrasound biomicroscope (Fig.1).

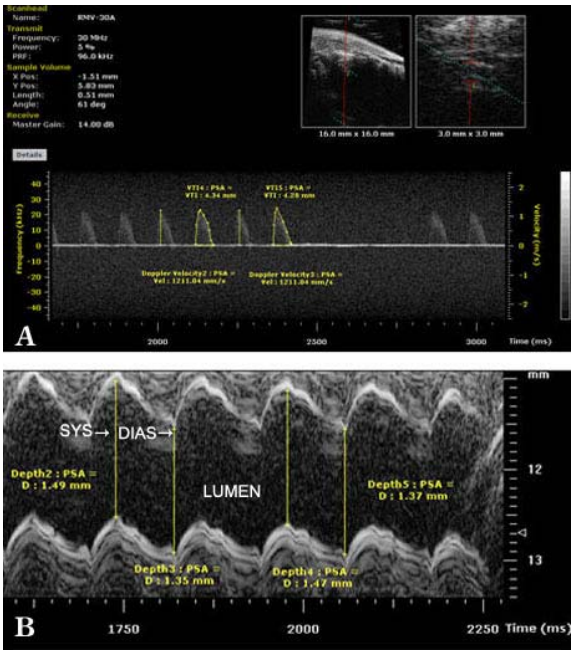

Fig. 1 Ultrasound measurement of the ascending aorta of a mouse using multifrequency ultrasound biomicroscope
(a) the flow in the ascending aorta and
(b) the diameter of the ascending aorta measured during systole and diastole of the cardiac cycle.
SYS = Systolic Phase, DIAS = Diastolic Phase.

2.2 Mouse Blood Viscosity Measurement

The protocol for blood viscosity measurement was modified from the International Committee for Standardization in Hematology (ICSH) Guidelines for Measurement of Blood Viscosity and Erythrocyte Deformability, 1986. The mice were systemically heparinized by injection (approximately 50-100 units) via the tail vein. Blood was taken from each mouse under general anesthesia with isoflurane (1-3% at 1-3 L/min) after 30 minutes of heparinization. The hair was

removed from the chests of the mice and the hearts were punctured percutaneously. About 0.5-1 ml of blood was drawn gently without contamination of hair, fat or tissue. The mice were then euthanized with carbondioxide inhalation. The samples were kept in one ml containers without heparin at 4 °C. Blood viscosity measurements were done on samples from individual mice.

A cone - plate type rheometer (AR 2000, TA Instruments, Newcastle, DE, USA), was used for blood viscosity measurements so that measurements could be made under controlled stress and shear. The measurements were done with the 40mm and/or 60 mm cones, which required blood volumes of 0.49 ml and 0.15 ml, respectively. The tests were performed either in the controlled stress and/or controlled strain mode, at 37 °C. Viscosity data were obtained at shear rates from 10 to 8,000 sec^{-1} within 6 hours after specimens were taken, and specimens were well mixed before rheological testing. The tests were repeated with the same and different geometries if there was an abnormal result.

2.3 Casting of the arterial tree

The casting was performed in each mouse. The left ventricle was canulated at the apex with angiocatheter no. 16. –19. The aorta was flushed with heparin saline to clear excess blood. The aorta was then injected with Batson's No.17 Plastic Replica (Polysciences, Inc. Warrington, PA. USA) through the left ventricle in order to replicate the in vivo geometry of the artery. The optimum technique for control of the polymerization is as follows: (a) Add 4 ml of Catalyst in Base Solution A 10 ml; Part I. (b) Add 4 drops of promoter C in Base solution A 10 ml; Part II. (c) Mix the Part II solution for 5 minutes. (d) Finally add Part I and Part II solutions together and stir to mix for 5 minutes. The complete compound was injected at a controlled pressure (100 –120 mmHg), and held at this pressure for 45 minutes and left for 24 hours. After the cast had completely polymerized, the aorta was dissected free from the perivascular tissue for pathology or put into saturated KOH solution for 48 hours and the resulting corrosion casts were then cleaned in distilled water and air dried.

2.4 Model Construction

In order to proceed with the computational flow modeling, a finite element model of each cast geometry was constructed. The basic steps used to construct a finite element model were as follows. The cast was scanned by Micro-Computerized Tomography scanning with a resolution of 17μm/ pixel. The 3-D image from the CT scan was segmented into a cross-sectional contour of the artery lumen using Amira 3.1 (Mercury Computer Systems / VSG Group, San Diego, CA). Each section of the CT scan result was reconstructed into three-dimensional model. The model was refined into a clean surface model (Fig. 2). The contour was used to reconstruct the arterial surface. Extensions were added to the great vessels and the descending aorta using standard techniques so as to ensure fully-developed flow at the vessel outlets**.** A surface triangulation was generated and imported using the Tetra meshing module of ICEMCFD (ICEM CFD Engineering, Berkeley, CA) and used to generate a tetrahedral finite element mesh, which was post-processed by adding nodes to give P_2-P_1 Taylor-Hood finite elements.

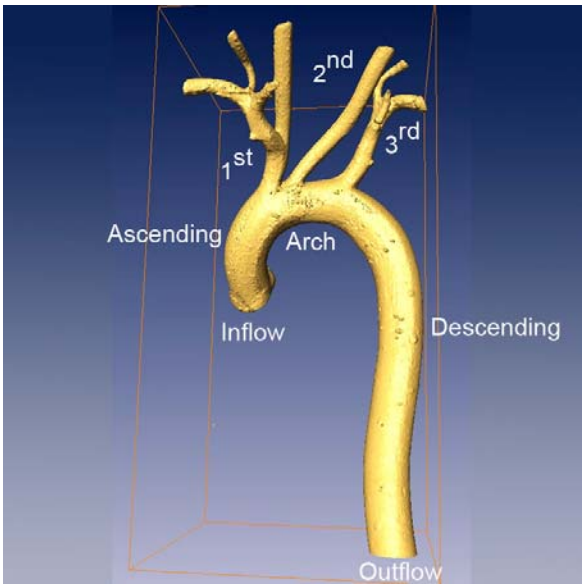

Fig. 2. Three-dimensional model of mouse aorta. The aortic arch is the curved continuation ascending aorta (Inflow) and gives three branches to supply the head and upper extremities. The aortic arch joins the descending aorta in the same plane as its origin from the ascending aorta.

2.5 Computational Fluid Dynamics

In this study, blood is assumed to be an incompressible Newtonian fluid and thus the stress – strain rate relations are described by the Newtonian model:

$$\sigma_{ij} = -p\delta_{ij} + \mu(\frac{\partial u_i}{\partial x_j} + \frac{\partial u_j}{\partial x_i}). \qquad (1)$$

The equations governing blood flow include the constitutive equations (1) and the following continuity equation and stress equations of motion,

$$\frac{\partial u_j}{\partial x_j} = 0, \qquad (2)$$

$$\rho\left(\frac{\partial u_i}{\partial t} + u_j \frac{\partial u_i}{\partial x_j}\right) = \frac{\partial \sigma_{ij}}{\partial x_j} + F_i, \qquad (3)$$

where u_i represents the component of velocity vector in the *i*th direction, p denotes pressure in the flow channel, μ and ρ denote respectively the blood density and the blood viscosity, and F is the body force acting on the fluid. By substituting equation (1) into (3), we obtain the following Navier-Stokes equations

$$\rho\left(\frac{\partial u_i}{\partial t} + u_j\frac{\partial u_i}{\partial x_j}\right) = F_i - \frac{\partial p}{\partial x_i} + \mu\frac{\partial}{\partial x_j}\left(\frac{\partial u_i}{\partial x_j} + \frac{\partial u_j}{\partial x_i}\right) \qquad (4)$$

Equation (4) together with the continuity equation (2) constitute a closed system of four partial differential equations, in terms of four coordinate and time-dependent unknown functions u_1, u_2, u_3 and p. To complete define the flow problem, we establish initial conditions that specify the value of the unknown function at t=0 second for all points in the domain:

$$u_1 = u_2 = u_3 = 0, \quad p = 0 \qquad (5)$$

and boundary conditions that specify the value of the unknown functions and/or its derivatives on the boundary of the domain for all time. For a typical mouse aortic arch, the boundary of the computation region consists of the inflow surface, the artery wall, and the outflow surfaces.

On the inflow surface, the velocity is set to the pulsatile velocity, $u_i = \tilde{u}_i$ as shown in Fig. 1. The no-slip condition is applied to the artery wall. On the outflow surfaces, the normal stress is specified:

$$\sigma_{ij} \cdot n = -p(t)n \qquad (6)$$

where n is the unit normal vector of the outlet surfaces and p(t) is the corresponding pulsatile pressure condition on the outlet surface of the computation region.

We now obtain the governing equations consisting of the differential equations (2) and (4) and all above boundary conditions to describe the fluid flow problem in a mouse aortic arch. To solve the fluid flow problem, let us put the equations in dimensionless form by choosing three characteristic quantities: characteristic length R (inlet radius) and the characteristic velocity U_0 (the mean inlet velocity). Using the following dimensionless variables

$$x_i^* = \frac{x_i}{R}, \quad t^* = \frac{U_0}{R}t, \quad u_i^* = \frac{u_i}{U_0}, \quad p^* = \frac{1}{\rho U_0^2}p, \quad F_i^* = \frac{R}{U_0^2}F_i \qquad (7)$$

and a dimensionless parameter, Reynolds number, as defined below

$$R_n = \frac{\rho U_0 R}{\mu} \qquad (8)$$

the continuity equation (2) and the Navier-Stokes equations (4) become

$$\frac{\partial u_j^*}{\partial x_j^*} = 0, \qquad (9)$$

$$\alpha^2\frac{\partial u_i^*}{\partial t^*} + R_n u_j^*\frac{\partial u_i^*}{\partial x_j^*} = R_n F_i^* - R_n\frac{\partial p^*}{\partial x_i^*} + \frac{\partial}{\partial x_j^*}\left(\frac{\partial u_i^*}{\partial x_j^*} + \frac{\partial u_j^*}{\partial x_i^*}\right) \qquad (10)$$

where α is the Womersley parameter defined by $\alpha = R\sqrt{\frac{\rho\omega}{\mu}}$ with $\omega = \frac{U_0}{R}$.

We now need to establish boundary conditions for the dimensionless problem. On the inflow

surface, the velocity is set to the dimensionless pulsatile velocity:

$$u_i^* = \tilde{u}_i^* \quad (11)$$

The no-slip condition is applied to the artery wall:

$$u_i^* = 0 \quad (12)$$

On the outflow surfaces, the normal stress is specified:

$$\sigma_{ij}^* \cdot n = -p^*(t)n \quad (13)$$

In summary, the fluid flow problem in a mouse aortic arch is governed by following dimensionless boundary value problem.

BVP: Find *u* and *p* such that the field equation (9) and (10) are satisfied in computation region and all boundary conditions (11)-(13) are satisfied.

A well-validated, in-house finite element code which solves the three dimensional Navier-Stokes equations was used to compute the wall shear stress and velocity patterns in the ascending aorta and the aortic arch. The non-dimensionalisation scheme is based upon the following characteristic quantities: length R (inlet radius); time ω-1 (inverse unsteady frequency in radians); velocity U_0 (spatial and temporal mean inlet velocity); and pressure ρU_0^2. Using these characteristics, the dimensionless Navier-Stokes equations take the following form:

$$\alpha^2 \frac{\partial u}{\partial t} + \mathrm{Re}\, u \cdot \nabla u = -\mathrm{Re}\, \nabla p + \nabla^2 u \quad (14)$$

$$\nabla \cdot u = 0 \quad (15)$$

where α, the Womersley parameter and Re, the Reynolds number

2.6 Histopathology

Pathology was examined in 15 apolipoprotein E knock-out mice (apoE-/-) and 12 normal mice. In order to remove the tissue from the cast, an incision was made at the posterior wall of the aorta longitudinally where there were no branches, using a scalpel blade. Firm pressure was applied to the scalpel to cut all layers of the artery. As a result, the incision left a mark on the cast which was useful for determining the tissue orientation later. Incisions were also be made along the branches. The tissue was then carefully removed from the cast in one piece. The whole aorta was used for *en face* lipid staining.

After the adventitia was removed, the aorta was cut open longitudinally and stained with oil red O to visualize the extent of the lipid deposition. Prior to sectioning the aorta, a detailed sketch of the cast was prepared to record the locations of the histological sections. The aorta was then cut at 3-5 mm intervals. The distal end of each cross-section was demarcated with black Indian ink so that the slides were cut consistently from the same side of the sections. Tissue blocks were sliced into 5-μm sections.

3 Results

3.1 Blood Viscosity

Blood from both apoE-/- and CD1 (normal) mice demonstrated the shear thinning properties. (Fig. 3.) For the apolipoprotein E knockout mice: the average blood viscosity was 3.33±0.45 (mean ± SD) mPa.sec at a shear rate of 1000 s^{-1}. For the normal mice group: the average blood viscosity was 3.48±0.39 (mean ± SD) mPa.sec at a shear rate of 1000 s^{-1}. There was no significant difference in the blood viscosity between the apoE-/- mice and the CD1 mice at shear rates of 10, 100, 1000, 3981 and 6310 s^{-1} (Table 1).

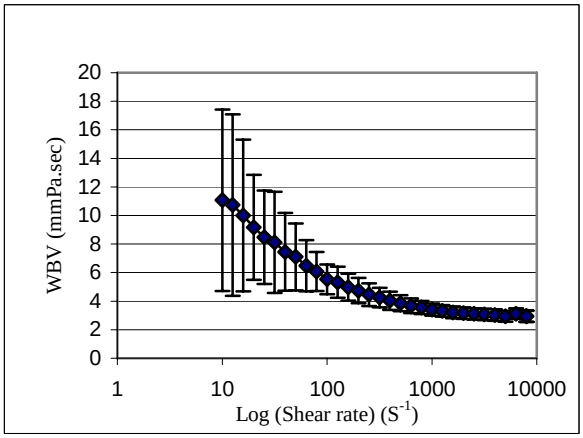

Fig. 3 Plot of average whole blood viscosity vs. shear rate in mice (combined apoE-/- and normal mice, 29 in number).
Bars represent the standard deviation.

Table 1 Comparison of blood viscosity between different types of mice (apoE-/- and CD1 mice) at different shear rates.

Shear Rate(s^{-1})	Mouse Type (n)	Blood Viscosity Mean ± SD (mPa.sec)	*P* value
10	apoE (16)	11.89 ± 8.27	0.437
	CD1 (12)	9.96 ± 1.93	
100	apoE (16)	5.44 ± 1.16	0.608
	CD1 (13)	5.64 ± 0.92	
1000	apoE (16)	3.33 ± 0.45	0.280
	CD1 (13)	3.50 ± 0.40	
3981	apoE (16)	2.99 ± 0.43	0.530
	CD1 (13)	3.09 ± 0.38	
6310	apoE (12)	3.11 ± 0.41	0.709
	CD1 (9)	3.17 ± 0.32	

3.2 Model 1

The calculated Reynolds number was 165. As this blood viscosity was found to be constant (for shear rate more than 1000 1/sec) we can therefore assume that blood behaves like a Newtonian fluid.

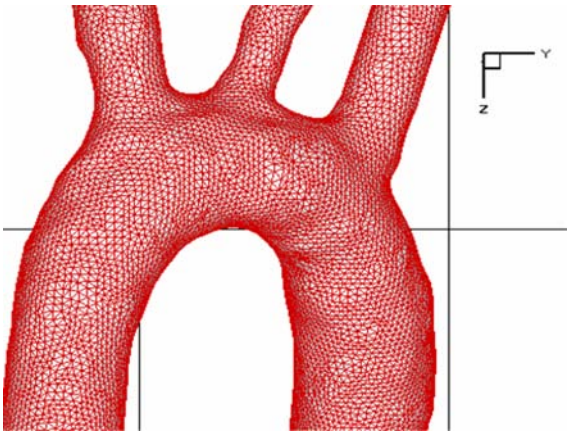

Fig. 4 Finite element mesh in mouse aortic arch. There were 167,918 nodes and 109,543 elements in the model.

Figure 4 shows a modeled three-dimensional aortic arch and distribution of finite elements. The model contained a total of 167,918 nodes with 109,543 elements. The wall boundary was assumed to be rigid and blood was modeled as an incompressible Newtonian fluid.

The magnitude of wall shear stress, relative to the inlet wall shear stress, is shown in Figure 5. Red represents high wall shear stress and blue represents the low wall shear stress area.

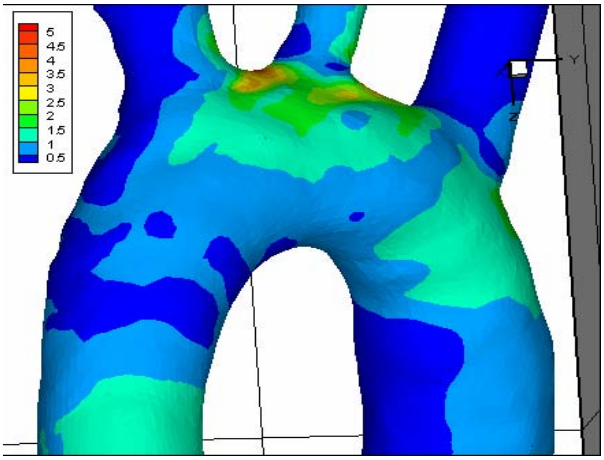

Fig. 5 The magnitude of wall shear stress in normal mice. Red represents high wall shear stress and blue represents the low wall shear stress area. All wall shear stress magnitudes were relative to the inlet wall shear stress.

The convergence history of computation is shown in Figure 6. Simulations were deemed to have converged in time when the normalized difference in the velocity field between two successive time steps, n and n-1, was no longer steadily decreasing. The difference, ε, was defined as:

$$\varepsilon = \frac{1}{\mathrm{Re}\,\Delta t}\frac{\sqrt{\sum_{i=1}^{3}\sum_{j=1}^{Ni}(u_{ij}^{n}-u_{ij}^{n-1})^2}}{N_1+N_2+N_3}$$

where u_{ij} denote the i^{th} component of the velocity vector for the j^{th} node, N_i is the number of non-Derichlet velocity nodes in the mesh for the i^{th} component of the velocity vector and Δt is the time step size.

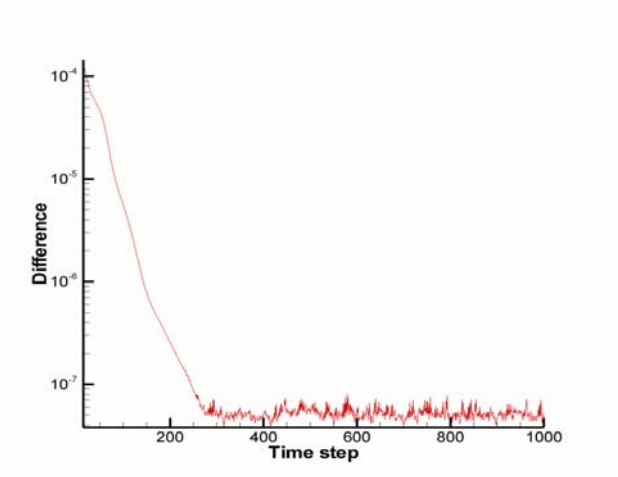

Fig. 6 The convergence history in flow simulation.

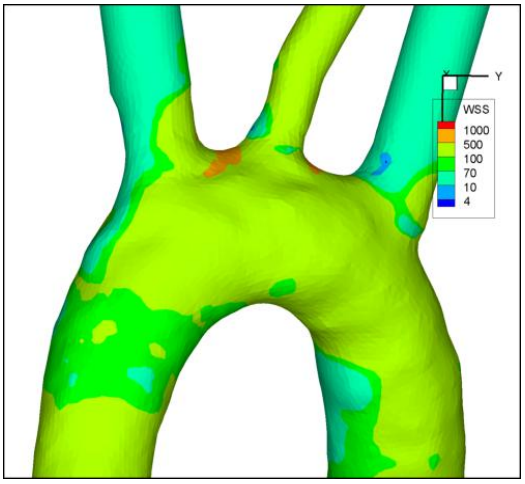

Fig. 7 The absolute wall shear stress in the aorta.

Fig. 6 shows the wall shear stress in dyne/cm^2. The calculated inlet wall shear stress was 182 dyne/cm^2. The plotting color represents actual wall shear stress distribution. The third branch has a dark blue area, indicating a very low wall shear stress.

3.3 Model 2

Another mouse model, Figure 8a, was used to calculate wall shear stress. The total number of nodes was 461,330 with 326,089 elements. The calculated Reynolds number was 140.91. Figure 8b demonstrated the actual wall shear stress plot. The calculated inlet wall shear stress was 110.55 dyne/cm^2. The first branch has a dark blue area, indicating a very low wall shear stress.

a.

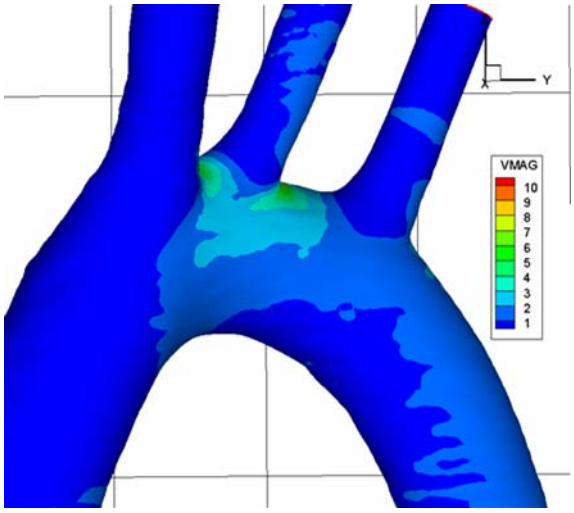

b.

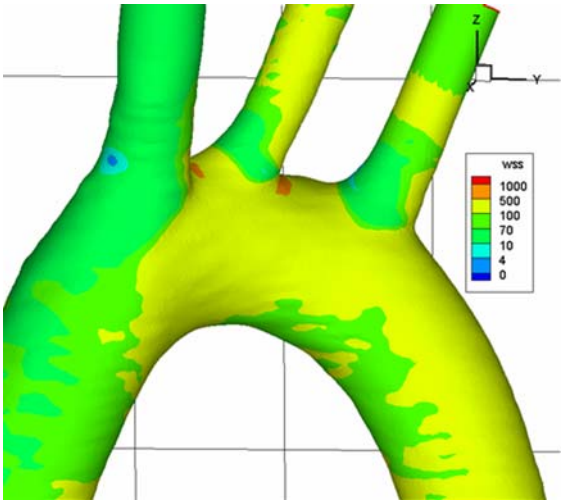

Fig. 8 a, The magnitude of wall shear stress. All wall shear stress magnitudes were relative to the inlet wall shear stress,
b, The absolute wall shear stress in the aorta.

3.3 Histopathology Results

There were 21 normal mice and 20 apoE knock out mice. Nine normal mice and 13 apoE -/- mice were fed the cholesterol diet. Only 27 mice had pathological examination (12 normal mice and 15 apoE-/- mice). Seven mice (46.7%) in the apoE-/- group developed atherosclerosis (6 in experimental group and one in control group) (Table 2). Atherosclerosis was found in 2 in each branch (2 in the first branch, 2 in the second branch and 2 in the third branch) (Table 3). There was no atherosclerosis found in the normal mice group in either control or experimental group.

Table 2 Pathological results in apoE-/-mice.

		Pathology		Total
		Positive	Negative	
Group	Experiment	6	4	10
	Control	1	4	5
Total		7	8	15

Table 3 Distribution of pathology in three branches of the aortic arch in apoE-/- mice.

	1st Branch	2nd Branch	3rd Branch
Positive	2	2	2
Negative	8	7	6
Total	10	9	8

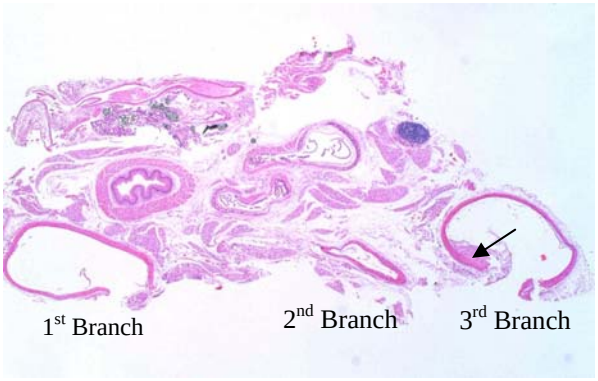

Fig. 9 Histopathology from atherosclerotic mice at 8 weeks after cholesterol fed demonstrated atherosclerosis (arrow) area in the third branch of the aortic arch.

H&E × 2.5 (original magnification)

Figure 9 shows the atherosclerotic lesion. There was increased intimal thickening of the third branch of the mouse aortic arch. This also corresponds to the area of lowest wall shear stress in Figure 6. The first and second branches were normal.

4 Discussion

The polypeptide apolipoprotein E (apoE) is important in the hepatic clearance of circulating cholesterol. When apoE is dysfunctional or absent, severe hyperlipidemia occurs in humans and in animal models. In apoE-knockout (apoE -/-) mice, atherosclerosis develops and progresses spontaneously, with lesions covering over 20% of the proximal aortic wall at 4 months and 50% at 13 months. Because the lesions progress with age and to some degree resembles human atherosclerotic lesions, apoE-knock out mice are considered a potentially important model of human atherosclerosis. Moreover, lesions in this animal can be accentuated by the use of a hypercholesterolemic diet. Numerous studies have been performed to characterize the morphology, pathology, and histology of arterial lesions in apoE -/- mice. However, alterations to other aspects of cardiac and vascular physiology and function have not been well characterized in this model. This study was able to evaluate and demonstrate the possibility of hemodynamic study and also the blood flow simulation in these transgenic mice.

Our study agrees with the previous studies that the atherosclerosis tend to occur at the low wall shear stress area [1-10]. However low wall shear stress alone was insufficient to cause the atherosclerosis as we did not find any atherosclerosis in normal mice even when a hypercholesterol diet was given. Our study demonstrated that genetics may play a more important role in the pathogenesis of atherosclerosis. Each mouse had slightly different vascular geometry. Therefore, there might be some differences in the wall shear stress distribution. This needs further investigation. Site-specific aortic lesion development found in our study was similar to reports in other pathological studies [11]. The future study would be the consideration of non-Newtonian blood viscosity, effect of changes of blood flow in cardiac cycle in the model, elasticity of artery and porous property of the arterial wall [12-14]. The imaging techniques with the micro CT scan or the magnetic resonance imaging might be improved for accuracy of obtained geometry and flow velocity measurement. The comparative study with the human flow parameters must be performed.

Fukushima T. *et al.* in 1985 studied the flow pattern in the dog aortic arch [15]. They found that flow disturbances observed in the aortic arch have characteristics similar to those of secondary flow, which is called the horseshoe

vortex, produced at Y- and T-junctions. The particles captured by the secondary flow near the flow divider, for instance, moved in a direction opposite or perpendicular to the mean flow. The vortex produced a typical stagnation region at the wall of the aorta just proximal to the branching site of the first and the third branches. When the rate of flow to a daughter branch decreased, separation of the flow occurred at the proximal outer wall of the branch artery. Endo S. *et al.* in 1996 studied flow patterns in dog aortic arch by means of flow visualization and high-speed cinemicrographic techniques, using transparent aorta [16]. Under a steady flow condition at inflow Reynolds numbers of 700-1600, which simulated physiologic conditions at early- to mid-systole, slow, spiral secondary, and recirculation flows formed along the left anterior wall of the aortic arch and at the entrance of each side branch adjacent to the vessel wall opposite the flow divider, respectively. The flow in the aortic arch consisted of three major components, namely, an undisturbed parallel flow located close to the common median plane of the arched aorta and its side branches, a clockwise rotational flow formed along the left ventral wall, and the main flow to the side branches, located along the right dorsal wall of the ascending aorta. Thus, looking down the aorta from its origin, the flow in the aortic arch appeared as a single helical flow revolving in a clockwise direction. Regions of low wall shear stress were located along the leading edge of each side branch opposite the flow divider where slow recirculation flows formed, and along the left ventral wall where slow spiral secondary flows formed. Barakat A. *et al*. in 1997 study the flow pattern in rabbit aorta [17]. The aortic arch exhibited a single cell of clockwise-rotating helical secondary flow along the ventral and inner walls. Flow separation occurred proximal to the two arch branches with the flow reversal proximal to the first arch branch. Sinusoidal flow rendered the helical motion more pronounced in systole, while the reverse flow zone periodically expanded and contracted. Engelbrecht H. *et al*. in 1998 found that the velocity field distribution was found to be uniform throughout the model during the time of increasing inlet velocities [18]. With decreasing inlet velocities a region of low flow developed in the descending portion of the model leading to recirculating flow at the inner wall. In this region of low flow the variation in velocity with time at the inner wall was approximately twice the variation at the outer wall. As a result of the recirculating flow, the wall shear stresses at the inner wall are low and oscillating, predisposing to the development of atherosclerosis. Del Gaudio C. *et al.* in 2006 studied the flow field in a realistic model of aortic arch [19]. They also applied a time dependent non-Newtonian characteristic in the study. The spatial shear stress pattern, within the cardiac cycle, was shown to have higher values in correspondence to the inner wall of the aortic arch and the sites where the major vessels originated from the arch itself. The velocity patterns, on transversal sections of the aorta, resulted in highly skewed morphology.

The blood flow in human aortic arch has been studied using magnetic resonance imaging. Kilner PJ. *et al.* used three-directional phase contrast cine magnetic resonance velocity mapping to map multidirectional flow velocities in the aortas of 10 healthy volunteers.[20] Right-handed helical flows predominated in the upper aortic arch in late systole, being clearly recognizable in 9 of the 10 subjects. Helical flow patterns in the upper descending aorta varied between subjects, apparently depending on arch curvature. End-systolic retrograde flow originated from regions of blood with low momentum, usually along inner wall curvatures. Markl M. *et al*. used Time-resolved, 3-dimensional phase-contrast magnetic resonance imaging (3D CINE PC MRI) to obtain complete spatial and temporal coverage of the entire thoracic aorta combined with spatially registered 3-directional pulsatile blood flow velocities [21]. They found a right-handed helix through the ascending aorta and a late systolic retrograde flow channel along posterior left aortic wall.

Shahcheraghi N. *et al.* studied a three-dimensional and pulsatile blood flow in a human aortic arch and its three major branches by a finite-volume formulation of the Navier-Stokes equations for a peak Reynolds number of

2500 and a Womersley parameter of 10 [22]. They found that the primary flow velocity is skewed towards the inner aortic wall in the ascending aorta, but this skewing shifts to the outer wall in the descending thoracic aorta. Within the arch branches, the flow velocities were skewed to the distal walls with flow reversal along the proximal walls. Within the aorta, wall shear stresses were highly dynamic, but were generally high along the outer wall in the vicinity of the branches and low along the inner wall, particularly in the descending thoracic aorta. Within the branches, the shear stresses were considerably higher along the distal walls than along the proximal walls. Wall pressure was low along the inner aortic wall and high around the branches and along the outer wall in the ascending thoracic aorta. Comparison of numerical results with the localization of early atherosclerotic lesions broadly suggests preferential development of these lesions in regions of extrema (either maxima or minima) in wall shear stress and pressure.

Suo J. *et al*. studied the relationship of wall shear stresses and atherosclerosis in wild-type mice [23]. They found that low wall shear stress areas which are along the inner curvature of the aortic arch and at the orifices of the arch branches are prone to develop atherosclerosis as in the human aorta.

The implications of this study are that it is necessary to understand the mechanistic role of hemodynamics in the pathogenesis of the aortic aneurysm/ aortic dissection and it may be useful in the design and development of aortic stents.

5 Conclusion

We conclude that flow simulation in the mouse aortic arch is feasible, however, extrapolation of the mouse aortic hemodynamic results to the human situation needs further study. Given that the transgenic mouse and humans have the same geometry of aorta as in the normal CD1 mouse, the wall shear stress in this study could be compared with the localized atherosclerotic lesions in previous studies. We also noted that the atherosclerotic lesions were found more frequently in the low wall shear stress areas as described in earlier pathology reports.

Acknowledgements

Deepest appreciation is extended to the Thailand Research Fund (contract number PHD/0202/2544) for financial support. We gratefully acknowledge Dr. Yu-Qing Zhou, Research Associate, Mouse Imaging Centre, The Hospital for Sick Children, The University of Toronto, for advice on the ultrasound biomicroscope; Dr. David Courtman, Saint Michael Hospital, Toronto for advice on vascular casting; Prof. David James, Department of Mechanical Engineering, University of Toronto for setting up the blood viscosity experiment; and Prof. C. Ross Ethier, Department of Mechanical Engineering, University of Toronto, for his guidance on computational fluid dynamic.

References:

[1] S. Mohan, N. Mohan, and E. A. Sprague, "Differential activation of NF-kappa B in human aortic endothelial cells conditioned to specific flow environments," *Am J Physiol*, vol. 273, pp. C572-8., 1997.

[2] M. Okano and Y. Yoshida, "Influence of shear stress on endothelial cell shapes and junction complexes at flow dividers of aortic bifurcations in cholesterol-fed rabbits," *Front Med Biol Eng*, vol. 5, pp. 95-120., 1993.

[3] A. Kirpalani, H. Park, J. Butany, K. W. Johnston, and M. Ojha, "Velocity and wall shear stress patterns in the human right coronary artery," *J Biomech Eng*, vol. 121, pp. 370-5., 1999.

[4] C. S. Lee and J. M. Tarbell, "Influence of vasoactive drugs on wall shear stress distribution in the abdominal aortic bifurcation: an in vitro study," *Ann Biomed Eng*, vol. 26, pp. 200-12., 1998.

[5] F. Inzoli, F. Migliavacca, and G. Pennati, "Numerical analysis of steady flow in aorto-coronary bypass 3-D model," *J Biomech Eng*, vol. 118, pp. 172-9., 1996.

[6] C. M. Gibson, L. Diaz, K. Kandarpa, F. M. Sacks, R. C. Pasternak, T. Sandor, C. Feldman, and P. H. Stone, "Relation of vessel wall shear stress to atherosclerosis

progression in human coronary arteries," *Arterioscler Thromb*, vol. 13, pp. 310-5., 1993.

[7] A. P. Sawchuk, J. L. Unthank, T. E. Davis, and M. C. Dalsing, "A prospective, in vivo study of the relationship between blood flow hemodynamics and atherosclerosis in a hyperlipidemic swine model," *J Vasc Surg*, vol. 19, pp. 58-63; discussion 63-4, 1994.

[8] Y. Yoshida, W. Sue, M. Okano, T. Oyama, T. Yamane, and M. Mitsumata, "The effects of augmented hemodynamic forces on the progression and topography of atherosclerotic plaques," *Ann N Y Acad Sci*, vol. 598, pp. 256-73, 1990.

[9] H. Yamawaki, S. Lehoux, and B. C. Berk, "Chronic physiological shear stress inhibits tumor necrosis factor-induced proinflammatory responses in rabbit aorta perfused ex vivo," *Circulation*, vol. 108, pp. 1619-25, 2003.

[10] H. M. Honda, T. Hsiai, C. M. Wortham, M. Chen, H. Lin, M. Navab, and L. L. Demer, "A complex flow pattern of low shear stress and flow reversal promotes monocyte binding to endothelial cells," *Atherosclerosis*, vol. 158, pp. 385-90, 2001.

[11] P. A. VanderLaan, C. A. Reardon, and G. S. Getz, "Site specificity of atherosclerosis: site-selective responses to atherosclerotic modulators," *Arterioscler Thromb Vasc Biol*, vol. 24, pp. 12-22, 2004.

[12] B. Wiwatanapataphee, S. Amornsamankul, Y. Wu, and Y. Lenbury, "Simulation of Transient Blood Flow through Stenosed Coronary Arteries," *WSEAS TRANSACTIONS on FLUID MECHANICS*, vol. 1, pp. 771-778, 2006.

[13] G. Liu, "Exact Variational Principles for Navier-Stokes Equations of 3-D Unsteady Viscous Flow," *WSEAS TRANSACTIONS on FLUID MECHANICS*, vol. 1, pp. 913-919, 2006.

[14] J. Svensson, R. Gardhagen, and M. Karlsson, "Assessment of Geometrical Influence on WSS Estimation in the Human Aorta," *WSEAS TRANSACTIONS on FLUID MECHANICS*, vol. 1, pp. 318-326, 2006.

[15] T. Fukushima, T. Karino, and H. L. Goldsmith, "Disturbances of flow through transparent dog aortic arch," *Heart Vessels*, vol. 1, pp. 24-8., 1985.

[16] S. Endo, Y. Sohara, and T. Karino, "Flow patterns in dog aortic arch under a steady flow condition simulating mid-systole," *Heart Vessels*, vol. 11, pp. 180-91, 1996.

[17] A. I. Barakat, T. Karino, and C. K. Colton, "Microcinematographic studies of flow patterns in the excised rabbit aorta and its major branches," *Biorheology*, vol. 34, pp. 195-221., 1997.

[18] H. Engelbrecht, C. M. Steinmann, and L. Pretorius, "Numerical simulation of pulsating flow in the aortic arch," *S Afr Med J*, vol. 88, pp. C40-3., 1998.

[19] C. Del Gaudio, U. Morbiducci, and M. Grigioni, "Time dependent non-Newtonian numerical study of the flow field in a realistic model of aortic arch," *Int J Artif Organs*, vol. 29, pp. 709-18, 2006.

[20] P. J. Kilner, G. Z. Yang, R. H. Mohiaddin, D. N. Firmin, and D. B. Longmore, "Helical and retrograde secondary flow patterns in the aortic arch studied by three-directional magnetic resonance velocity mapping," *Circulation*, vol. 88, pp. 2235-47, 1993.

[21] M. Markl, M. T. Draney, M. D. Hope, J. M. Levin, F. P. Chan, M. T. Alley, N. J. Pelc, and R. J. Herfkens, "Time-resolved 3-dimensional velocity mapping in the thoracic aorta: visualization of 3-directional blood flow patterns in healthy volunteers and patients," *J Comput Assist Tomogr*, vol. 28, pp. 459-68, 2004.

[22] N. Shahcheraghi, H. A. Dwyer, A. Y. Cheer, A. I. Barakat, and T. Rutaganira, "Unsteady and three-dimensional simulation of blood flow in the human aortic arch," *J Biomech Eng*, vol. 124, pp. 378-87, 2002.

[23] J. Suo, D. E. Ferrara, D. Sorescu, R. E. Guldberg, W. R. Taylor, and D. P. Giddens, "Hemodynamic shear stresses in mouse aortas: implications for atherogenesis," *Arterioscler Thromb Vasc Biol*, vol. 27, pp. 346-51, 2007.